Essential Readings in Light Metals: Aluminum Reduction Technology.
Edited by Geoff Bearne, Marc Dupuis and Gary Tarcy.

MAGNETOHYDRODYNAMIC EFFECT OF ANODE SET PATTERN ON CELL PERFORMANCE

M. Segatz, Ch. Droste and D. Vogelsang

VAW Aluminium-Technologie GmbH

53117 Bonn, Germany

Abstract

Numerical simulation of coupled bath/metal magnetohydrodynamics (MHD) and MHD stability analysis allow the optimization of anode set pattern with respect to minimal cell disturbance. The contribution of anode gas-induced forces and the impact on the flow field are discussed.

During a complete anode set cycle, the anode current distribution changes significantly due to varying anode resistances, frozen bath and different metal pad heights. Typically the largest disturbance to cell stability occurs during a short time span after the anode change. With steady-state MHD simulations immediately before and after each anode change - following the sequence of the underlying set pattern - the relevant cell current and ACD distribution are determined. The impact of these parameters on cell stability is predicted with a linear MHD stability analysis for a complete anode change cycle.

Introduction

Most modern aluminum reduction cells are based on technology which uses discontinuous prebaked anodes. Despite all the advantages of this technology, a major drawback is in the regular disturbance of the cell caused by the anode changes. The cell's thermal balance and electric current flow are both affected and need several hours to revert to normal conditions.

The thermal aftermath of an anode change on temperatures in the bath, liquid metal, new anode, and neighbouring anodes can be analyzed via measurements, or by means of transient thermal simulations. The current pick-up of a newly set anode takes several hours and can be easily determined by current measurements. It has been shown, and is well known to operational staff, that optimizing the anode setting height can shorten the time needed for the new anode to reach the nominal current and give improved cell performance [1].

An anode change in cells with an unfavourable magnetic field is often accompanied or followed by voltage instabilities. The change of the current flow distribution, due to the high resistance of the new anode, modifies the magnetic field and Lorentz forces in the liquid bath and metal and can lead to a situation where self-exciting MHD oscillations grow. This phenomenon known as "metal pad roll" is harmful as the cell voltage usually has to be increased to stabilize the cell resulting in a higher bath resistance. Besides the increased specific energy consumption, the thermal balance of the cell is influenced also by this measure.

For some cell technologies, it is noticable that the location of the changed anode has an impact on the tendency towards instability. This can be detected in higher noise values after these anodes have been changed. If the process control responds with a voltage increase to damp the noise, higher temperature values are sometimes correlated with specific anode changes. This effect, however, is usually difficult to detect because of the strong influence of AlF_3-concentrations on bath temperature.

In those cases where the current pick-up of a newly set anode is rather slow and takes longer than the time span of successive anode changes, an additional amplification of disturbances can occur. Depending on the sequence of anode changes, the current pick-up characteristic of the individual anodes and the deformation of the metal pad surface, a complicated current flow distribution can result either in a high or low MHD stability.

Transient magnetohydrodynamic simulations allow insights into the interaction between current flow, magnetic field, metal and bath flow, and metal pad deformation [2,3,5]. The underlying computational-fluid-dynamics (CFD) codes use a brute force approach to integrate the appropriate differential equations with respect to time. This approach, however, requires huge amounts of computer resources and is unsuitable for simulating a complete anode change pattern.

Operational procedures can be optimized, however, by coupling steady-state MHD simulations, before and just after an anode change, with the MHD stability analysis for each anode changed. The capability to predict the tendency towards metal pad roll for arbitrary cell technologies and sophisticated boundary conditions by means of a linear MHD stability analysis enables the straightforward optimization of cell design [6]. The linear stability analysis is used here to predict the impact of different anode change patterns on cell performance.

The basic idea of improving the anode set pattern based on MHD stability is to avoid high instability peaks and time spans with successively higher than average noise values during the set cycle. An accumulation of disturbing influences on the current distribution, and thus longer periods with many instabilities, should be avoided.

Besides the Lorentz forces, the gas bubble release has some influence on the movement of the bath and potentially on the liquid metal. This again changes the shape of the metal pad surface. As the MHD stability strongly depends on the distribution of the ACD, it is not clear, whether the gas bubble release influences the MHD stability or not. A comparison of calculations with and without the inclusion of forces simulating the release of gas bubbles will give an answer.

MHD Stability Analysis of Anode Set Pattern

An analysis of an anode set pattern determines the MHD stability just after each anode change. This is the moment when the largest MHD disturbance of the cell can be expected, as the new anode carries the minimum current and the largest horizontal current density in the liquid metal occurs. This corresponds to the well-known fact that instabilities are most often detected soon after the change of an anode.

For each anode to be changed the cell state just before the new anode set has to be determined first. The current distribution, the metal pad surface as well as the height and shape of the anode bottom sides have to be described in detail. This can be done by taking the data from a steady-state simulation of an undisturbed cell with uniform anodic currents. A more precise approximation involves the resistance distribution of all anodes according to their individual age and the determination of a corresponding current distribution. In both cases, it is assumed that the anode bottom side is burned long enough to reflect the shape of the metal pad surface. This first calculation is performed with a modified CFD package from CHAM, Inc. known as "ESTER" [4,5]. The result of this simulation is a consistent 3-D, steady-state solution for the cell including the 3-D distribution of metal and bath movement, metal pad deformation, current flow, magnetic field and Lorentz forces. Electric induction, magnetic field of horizontal currents and burn of the anode bottom side are included as well.

A second run with the ESTER package determines the cell state just after the anode change. It is assumed here that the cell has already reached a new quasi steady-state with a new distribution of metal and bath movement, metal pad deformation, current density, and magnetic field. This ESTER run differs in two ways from the first run. Firstly, the electric resistance of the new set anode is set to a large value to allow only about 10% of the nominal current to enter the new anode. And secondly, the shape of the anode bottom side is fixed and not determined by the local current density. Due to the modified current distribution, the anode bottom shape will reach a new steady-state after some hours, and this again will homogenize the ACD and the current distribution. At the moment of the largest disturbance, however, the anode bottom shape has not responded to the changed current distribution.

It should be mentioned that freezing of the bath along the bottom and side of the anode is not modeled here. Some hydrodynamic effect of blocks of frozen bath can be expected. The size and shape of these regions, however, are very uncertain. It was preferred to disregard this effect.

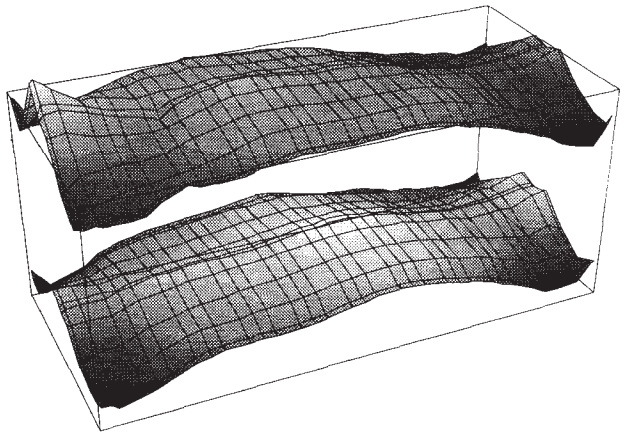

Figure 1: Metal pad surface before (bottom) and after (top) change of the anode in the front left-hand corner.

An example of the change of the metal pad surface after an anode change is given in Figure 1. For an older and magnetically uncompensated 165-kA end-to-end cell in the VAW's Rheinwerk smelter, the metal pad deformation is presented as inflated topology just before the change of the front left-hand corner anode (bottom) and after the anode change (top). After the anode change, the metal pad surface is depressed in the central area of the cell and a high crest appears in the center channel in the vicinity of the newly set anode. This change in the metal pad defor-

mation is mainly due to additional Lorentz forces in the liquid metal. These are caused by the interaction of the magnetic field and horizontal currents flowing into the region below the changed anode.

The ACD distribution shows more valuable information with respect to the stability of the cell than the metal pad deformation, as it reflects the local bath resistances directly. Figure 2 presents the ACD distribution of the complete anode set cycle of the same Rheinwerk cell. The black rectangle indicates the position of the newly set anode in the sequence of an older anode change pattern. The mean ACD is 50 mm and varies from 5 mm (black) to 70 mm (white).

Small ACD values below a newly set anode are not critical as the current density in this area is small. Small ACD values often occur, however, on one side of the newly set anode, and larger ACD's on the other side. Depending on the direction of the vertical magnetic field the horizontal currents in the liquid metal flow towards the newly set anode causing clockwise or counterclockwise forces around said anode. These forces are responsible for the smallest ACD values and are a major influence on the MHD stability of the cell.

The flow direction of the liquid metal is also strongly affected by the anode changes - see Figure 3. The velocity patterns vary significantly after each anode change and at least for the cell technology analyzed here, it can be assumed that the metal pad movement is in a non-steady state for a large fraction of the anode set cycle time.

The current flow and ACD distribution of the second ESTER run and the electric resistances of all anodes are fed into the linear MHD stability analysis to determine the instability value for a specific anode change. The basics of the MHD stability code are described in [6].

The complete 3-D current flow and magnetic field distribution from the ESTER run is taken as steady-state. The ACD distribution and individual anode resistances are used in the electric potential equation, which is part of the eigenvalue problem determining the oscillation modes.

The distribution of the magnetic-to-kinetic energy transfer in the metal for the most unstable mode of each anode change is shown in Figure 4. The local origin of the instability mode is indicated by large values of transferred energy. As in the first example in [6], the same type of cell was analyzed there. The largest transfer values are always found in the back left- and front right-hand corners. For numbers 1 to 5 and 19 and 20 in the anode change cycle, however, the regions of large energy transfer are significantly smaller.

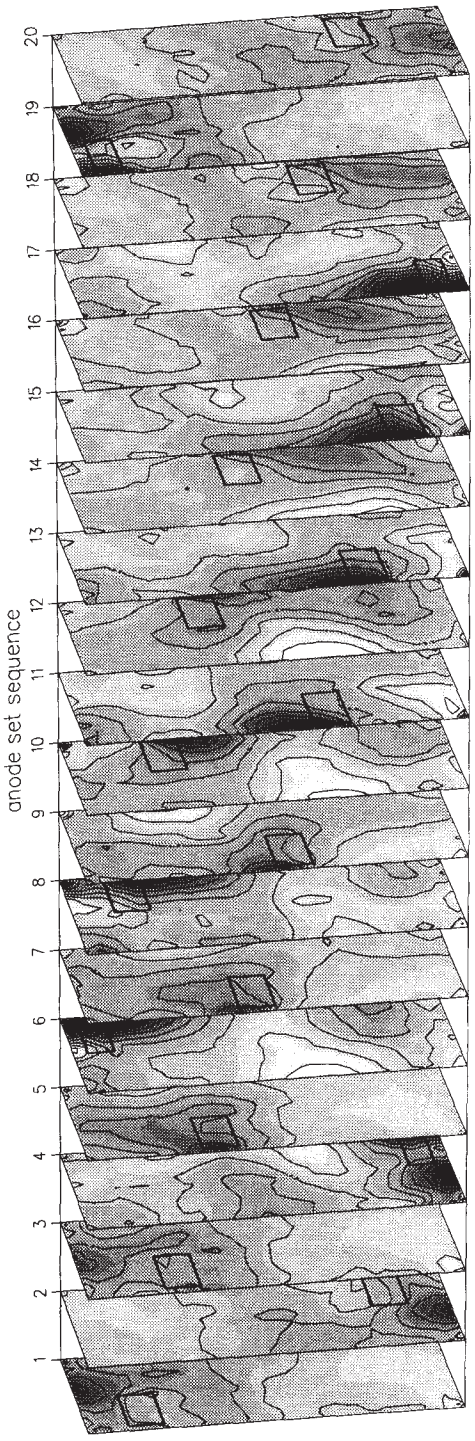

Figure 2: ACD distribution during a complete anc change cycle (20 anodes). State just after ea anode change is shown. Black areas are less th 5 mm ACD, white is more than 70 mm. Me ACD is 50 mm. In most cases, the smallest AC occurs close to the position of the changed anc (rectangle).

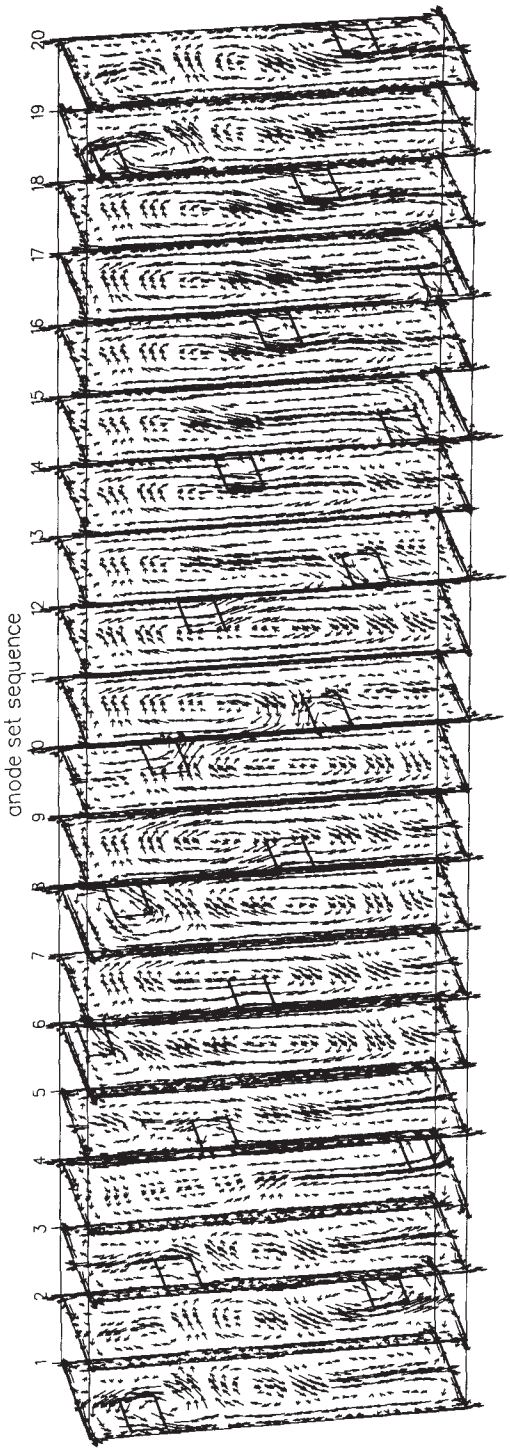

Figure 3: Metal flow distribution during a complete anode change cycle. Arrow length represents velocity. Flow pattern strongly depends on the position of the changed anode (rectangle).

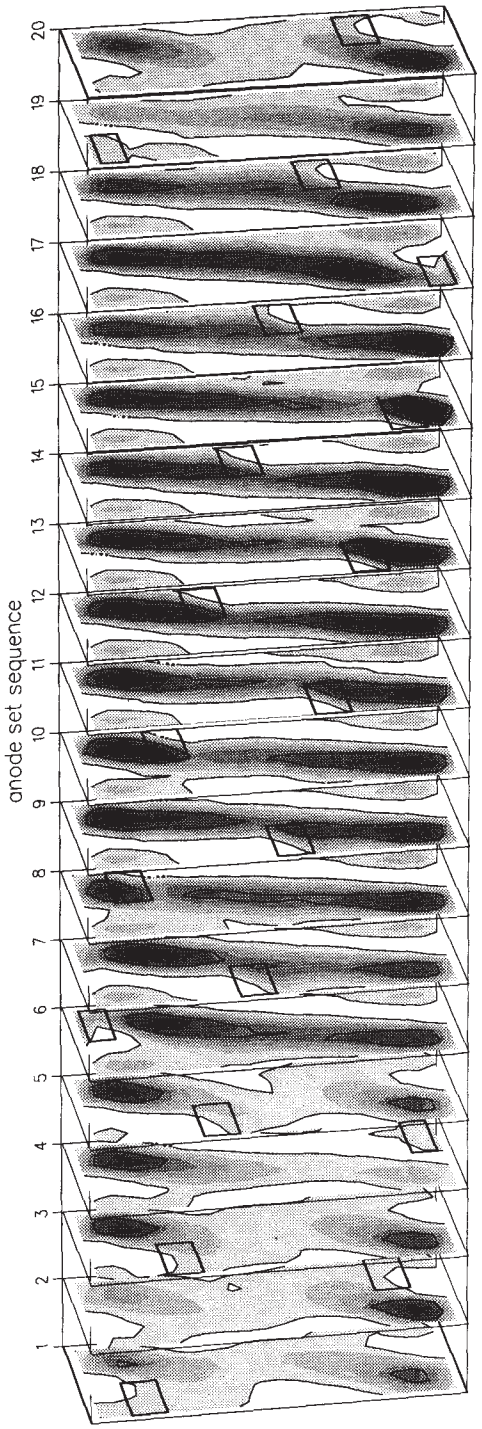

Figure 4: Magnetic-to-kinetic energy transfer during a complete anode change cycle. Values are from 0 (white) to 0.1 W/m^3 (black). The maximum energy transfer always occurs at similar locations and does not follow the position of the changed anode. Largest energy transfer occurs at anode change 6 to 18.

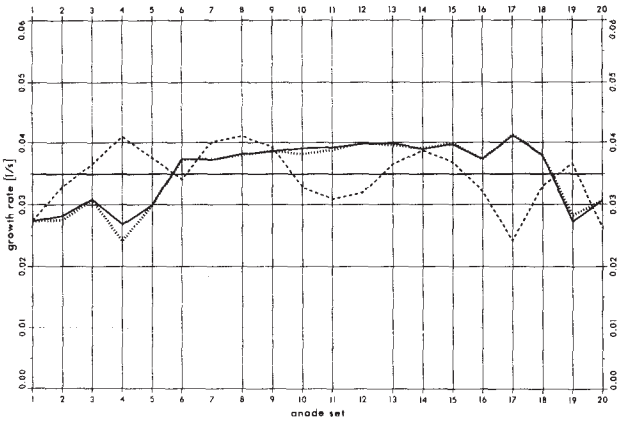

Figure 5: Growth rates of MHD instabilities for the two different anode set pattern (solid and dashed line). Results marked by the dotted line include the effect of gas bubble release for the first analyzed anode set pattern. The growth rate of the undisturbed cell is given by the horizontal line. Higher growth rates indicate a more unstable cell with higher noise values.

The growth rate indicates the tendency towards MHD instability. Figure 5 shows the change of growth rate during a complete anode set cycle (solid curve). Again, the cell shows maximum stability during the change of anodes 1 to 5 and 19 and 20.

The most unstable values correspond to anode changes in the back left- and front right-hand quarter of the cell. In these cases the horizontal currents in the liquid metal support the oscillation mode preferred by the vertical magnetic field. This corresponds to a superposition of type 1 and type 2 instabilities as explained in Figure 2 in [6]. There is no indication that the areas of small ACD in the vicinity of a newly set anode are responsible for an increased magnetic-to kinetic energy transfer.

Optimization of Anode Set Pattern

Because of the huge number of theoretical anode set pattern combinations, (n-1)! pattern for n anodes, it is impossible to analyze all of them with respect to MHD instability. The following approach was used to find those patterns which are likely to be favourable.

The method described here consists of three steps:

1. A sensitivity analysis determines the individual impact of a newly set anode on MHD instability. As described in the previous section, a complete MHD stability analysis is performed for each anode to be changed, with the assumption that the cell is in an undisturbed state just before each anode change. This fits with the assumption that every new anode picks up the nominal current at the time when the next anode is changed. The initial condition for each anode change is read from the steady-state solution of a cell with homogeneous current distribution. Because there is no interaction of successive anode changes, this gives an indication of which anode change will most likely disturb the cell stability.

2. Based on the sensitivity values achieved in Step 1, all combinations of possible anode set patterns are preliminarily rated. The consecutive change of anodes with high instability values, adjacent anodes or corner anodes gives low rates. Operational restrictions and defaults, such as the alternate change of anodes on up- and downstream side or pairs of anodes, are considered and usually reduce the number of possible anode set patterns significantly.

3. A complete MHD stability analysis of the 10 anode set pattern with the best ratings yields detailed information on the performance of the various patterns and allows a final ranking. In this step measured anode current pick-up curves are used to estimate the anode resistance curve.

The dashed curve in Figure 5 gives an example of a modified anode set pattern, where the former plateau of high instability values has been avoided.

Effect of Gas Bubbles

The most straightforward approach including the effect of gas bubbles would be to use a two-phase fluid simulation. Although, in principle, the CFD code ESTER is capable of simulating two-phase flows, calculations with gas bubbles did not converge numerically. Therefore, the influence of gas bubbles was approximated by surrounding each anode with a region of upward directed forces. No gas bubble forces were added below the anode since it is unlikely that the low velocity of drifting bubbles will transfer significant amounts of kinetic energy in this area.

The region with gas bubble forces is 3 cm thick, which is identical to the thickness of the inter-anode gap. The value of the upward force density was determined by means of a simulation of the same problem without any Lorentz forces. With a constant force density of 200 N/m^3, a velocity pattern very similar to the figures of bath flow with the effect of bubble release in [9] was found. The maximal value calculated here for the bath movement is 35 cm/s. This value is somewhat higher than given in [8] and [9]. It is reasonable to assume that a prescribed force density of

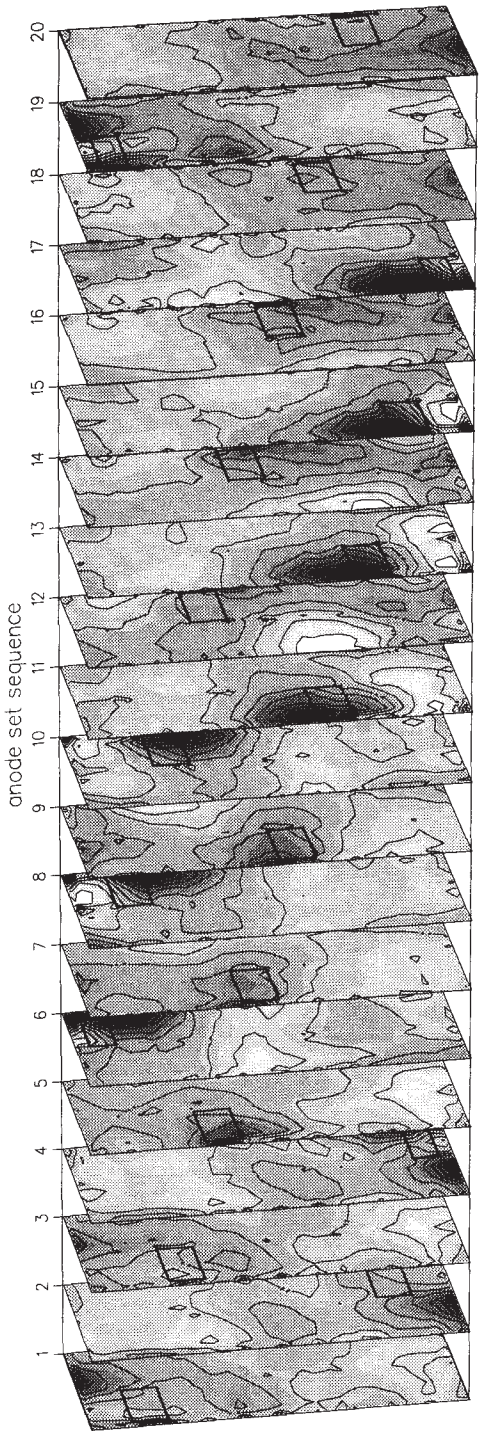

Figure 6: ACD distribution as in Figure 2 including the effect of gas bubble release.

200 N/m^3 for the gas bubble rise zone represents a worst case assumption with respect to gas bubble effects.

Figure 6 shows the ACD including the bubble release effects for the complete anode set cycle. Compared to Figure 2, without bubble release, only small changes can be seen. This does not mean that the metal pad surface shapes are similar. It can only be concluded that the change of the metal pad surface due to the current flow redistribution after anode change does not depend significantly on gas bubble release. The instability curves therefore with and without bubble release effect are nearly identical (dotted curve in Figure 5).

Conclusion

Coupling of steady-state MHD simulations with a linear stability analysis allows the determination of coherence between anode changes and MHD instability. The state of the cell before and just after each anode change is determined in a consistent manner. It gives valuable information on the change of metal pad surface and metal/bath movement. The MHD stability analysis can identify anode positions where an anode change affects the stability more than others. A correlation between noise values and instability prediction was found.

A crest in the metal pad is often formed after an anode change under one of the adjacent anodes. This increases the local current density; this effect, however, is seldom responsible for higher instability values. The strongest influence on stability comes from the horizontal currents compensating the current deficiency below the changed anode in the metal pad. In case of a magnetic uncompensated cell, the most unstable situation occurs if the horizontal currents in the liquid metal support the oscillation mode preferred by the magnetic field.

An optimization of the anode change pattern based on the target to avoid peaks of high instability and longer periods of excessive instability is possible. First of all, the huge number of conceivable anode pattern combinations has to be reduced by means of a sensitivity analysis and rating system before the most preferred pattern can be analyzed completely by an MHD analysis.

No effect of gas bubble release on liquid metal flow, ACD distribution and instability values was found. Although the consideration of gas bubble release by means of a vertical upward force around each anode is not perfect, this method allows a worst case approximation and in our simulations indicated that this term can be neglected for MHD instability purposes.

References

[1] A. Valles, G. Aiquel, and R. Craig, *Anode Setting Height Optimisation*, Light Metals 1991, 479-482.

[2] W.E. Wahnsiedler, *Hydrodynamic Modeling of Commercial Hall-Heroult Cells*. Light Metals 1987, pp.

269-287.

[3] V. Potocnik, *Modelling of Metal-Bath Interface Waves in Hall-Heroult Cells using ESTER/PHOENICS*. Light Metals 1989, pp. 227-235.

[4] H.I. Rosten, *The Mathematical Foundation of the ESTER Computer Code*. CHAM TR/84, 1982.

[5] M. Segatz, D. Vogelsang, C. Droste, and P. Baekler, *Modelling of transient magneto-hydrodynamic phenomena in Hall-Heroult cells*, Light Metals 1993, 361-368.

[6] M. Segatz and C. Droste, *Analysis of Magneto-hydrodynamic Instabilities in Aluminium Reduction Cells*, Light Metals 1994, pp. 313-322.

[7] M. Segatz and D. Vogelsang, *Effect of Steel Parts on Magnetic Fields in Aluminum Reduction Cells*. Light Metals 1991, pp. 393-398.

[8] J.M. Purdie et al., *Impact of Anode Gas Evolution on Electrolyte Flow and Mixing in Aluminium Electrowinning Cells* . Light Metals 1993, pp. 355-360.

[9] M.M. Bilek, W.D. Zhang and F.J. Stevens, *Modelling of Electrolyte Flow and its Related Transport Processes in Aluminium Reduction Cells*. Light Metals 1994, pp. 323-331.